Monthly Notices
of the
ROYAL ASTRONOMICAL SOCIETY

MNRAS **433,** 560–570 (2013)
Advance Access publication 2013 June 6

doi:10.1093/mnras/stt749

The 2011 October Draconids outburst – I. Orbital elements, meteoroid fluxes and 21P/Giacobini–Zinner delivered mass to Earth

Josep M. Trigo-Rodríguez,[1,2]★ José M. Madiedo,[3,4] I. P. Williams,[5] Joan Dergham,[1] Jordi Cortés,[1] Alberto J. Castro-Tirado,[6] José L. Ortiz,[6] Jaime Zamorano,[7] Francisco Ocaña,[7] Jaime Izquierdo,[7] Alejandro Sánchez de Miguel,[7] Jacinto Alonso-Azcárate,[8] Diego Rodríguez,[9] Mar Tapia,[10] Pep Pujols,[11] Juan Lacruz,[12] Francesc Pruneda,[13] Armand Oliva,[14] Juan Pastor Erades[14] and Antonio Francisco Marín[15]

[1] *Institute of Space Sciences (CSIC), Campus UAB, Facultat de Ciències, Torre C5-parell-2ª, E-08193 Bellaterra, Barcelona, Spain*
[2] *Institut d'Estudis Espacials de Catalunya (IEEC), Edif. Nexus, c/Gran Capità, 2-4, E-08034 Barcelona, Spain*
[3] *Facultad de Ciencias, Universidad de Huelva, E-21070 Huelva, Spain*
[4] *Departamento de Física Atómica, Molecular y Nuclear, Facultad de Física, Universidad de Sevilla, E-41012 Sevilla, Spain*
[5] *School of Physics and Astronomy, Astronomy Unit, Queen Mary, University of London, London, UK*
[6] *Instituto de Astrofísica de Andalucía (IAA-CSIC), Granada, Spain*
[7] *Departamento de Astrofísica y CC. de la Atmósfera, Facultad CC Físicas, Universidad Complutense de Madrid (UCM), Madrid, Spain*
[8] *Universidad de Castilla-La Mancha (UCLM), Toledo, Spain*
[9] *Guadarrama Observatory (MPC458), Madrid, Spain*
[10] *Laboratori d'Estudis Geofísics Eduard Fontseré (LEGEF), Institut d'Estudis Catalans, Barcelona, Spain*
[11] *Grup d'Estudis Astronòmics (GEA) and Agrupació Astronòmica d'Osona, Barcelona, Spain*
[12] *La Cañada Observatory, Ávila, Spain*
[13] *Astronomia des de l'Empordà, Palamós, Spain*
[14] *Agrupació Astronómica de Sabadell (AAS), C/Prat de la Riba s/n, E-08200 Sabadell, Barcelona, Spain*
[15] *Urb. Villapalma 10, 1º D, E-11203 Algeciras, Cádiz, Spain*

Accepted 2013 April 28. Received 2013 April 24; in original form 2012 November 16

ABSTRACT

On 2011 October 8, the Earth crossed the dust trails left by comet 21P/Giacobini–Zinner during its 19th and 20th century perihelion approaches with the comet being close to perihelion. The geometric circumstances of that encounter were thus favourable to produce a meteor storm, but the trails were much older than in the 1933 and 1946 historical encounters. As a consequence the 2011 October Draconid display exhibited several activity peaks with Zenithal Hourly Rates of about 400 meteors h^{-1}. In fact, if the display had not been forecasted, it could have passed almost unnoticed as was strongly attenuated for visual observers due to the Moon. This suggests that most meteor storms of a similar nature could have passed historically unnoticed under unfavourable weather and Moon observing conditions. The possibility of obtaining information on the physical properties of cometary meteoroids penetrating the atmosphere under low geocentric velocity encounter circumstances motivated us to set up a special observing campaign. Added to the Spanish Fireball Network wide-field all-sky and CCD video monitoring, other high-sensitivity 1/2 arcsec black and white CCD video cameras were attached to the modified medium-field lenses for obtaining high-resolution orbital information. The trajectory, radiant and orbital data of October 16 Draconid meteors observed at multiple stations are presented. The results show that the meteors appeared from a geocentric radiant located at $\alpha = 263.0 \pm 0.^{\circ}4$ and $\delta = +55.3 \pm 0.^{\circ}3$ that is in close agreement with the radiant predicted for the 1873–1894 and the 1900 dust trails. The estimated mass of material from 21P/Giacobini–Zinner delivered to Earth during the 6 h outburst was around 950 ± 150 kg.

Key words: comets: individual: 21P/Giacobini-Zinner – interplanetary medium – meteorites, meteors, meteoroids.

★ E-mail: trigo@ice.csic.es

1 INTRODUCTION: THE 2011 OCTOBER DRACONID OUTBURST

Meteor storms are quite unusual, but magnificent displays of nature that remind us of the crucial role that the terrestrial atmosphere can play in shielding us from direct impacts by interplanetary particles (Lovell 1954). Meteoroids with sizes over ∼100 μm typically ablate in the atmosphere where some of the kinetic energy generates a visible trail, a meteor (McKinley 1961). Because of the effects of perspective, when observed from the ground meteors seem to fall in their hundreds over a very short time-scales of minutes or even seconds (Fig. 1). As well as being spectacular, the study of meteor storms can be of great scientific value. From multistation recordings of meteors the velocity, deceleration and dynamic strength of the meteoroid can be measured, while from the radiant and the deduced velocity their heliocentric orbits can be calculated.

From an astrobiological perspective, the encounter of our planet with dense meteoroid streams under favourable geometric circumstances can also provide a unique opportunity to quantify the delivery of volatile-rich materials to Earth. At the present time, these rare encounters represent a sample of the delivery of organic molecules and water that were common in the past. These mechanisms could have participated in the terrestrial enrichment in volatiles at the time of the late heavy bombardment (Gomes et al. 2005). At that epoch fragile bodies were scattered by Jupiter and Saturn from the Kuiper Belt and the outer Main Belt disc, crossing the orbits of the terrestrial planets and experiencing regular close encounters. Direct impacts probably occurred, and could have been a key source of volatiles to Earth, but fragmentation of these ice-rich bodies in dust trails could have open additional pathways (Trigo-Rodríguez & Martín Torres 2013).

Though ancient written records of meteor storms are common, it is difficult to infer the fluxes of meteoroids to Earth from such historical reports because until the 20th century meteor observing was not standardized (Jenniskens 2006). The best ancient meteor reports provided the hourly rates but with hardly any information on cloud cover or the state of the moon. Despite the difficulties in interpreting the observations, past civilizations observed the skies in far better sky conditions than we do, but they were not able to understand what was being observed. Now, the meteor rate registered hourly by visual observers is standardized as the Zenithal Hourly Rate (ZHR). The ZHR corrects for several effects such as the zenith distance of the radiant, the stellar limiting magnitude (Lm) and the percentage of sky covered by clouds.

With modern techniques, the recording of meteor storms and computing the ZHR can be carried out to a level of high accuracy. In general, a shower is called a meteor storm if the ZHR exceeds 1000 meteors h^{-1}. In contrast, the sporadic meteor rate is usually less than 10 h^{-1}. In perfect conditions, with the radiant at the zenith, no obstacles and +6.5 limiting stellar magnitude with the naked eye, such a ZHR corresponds to a meteor frequency of about 1 meteor every 4 s. Such a rate will produce an obvious meteor display that can be seen even by inexperienced sky observers. Several comets are known to produce meteor storms, and 21P/Giacobini–Zinner is one of them. On 1933 October 9, a Catalan astronomer Josep Comas Solà observed one of the most intense storms and described it in a famous popular book: 'from the beginning of the night until 22 h, at least tens of thousands of meteors were observed over all Europe' (Comas Solà 1939).

Until the arrival of modern computers, meteor storm forecasting was a difficult task. Meteor storms are produced by tiny particles with typical sizes of tens or hundreds of microns that were released from a comet nucleus. The emission is driven by the sublimation of ices (Whipple 1951). As the orbits of the dust particles differ by a small amount from that of the parent comet, they will have slightly different orbital periods so that over time meteoroids will spread all around the orbit so that a meteor shower can be observed every year. (For a description of all the physics and mathematics

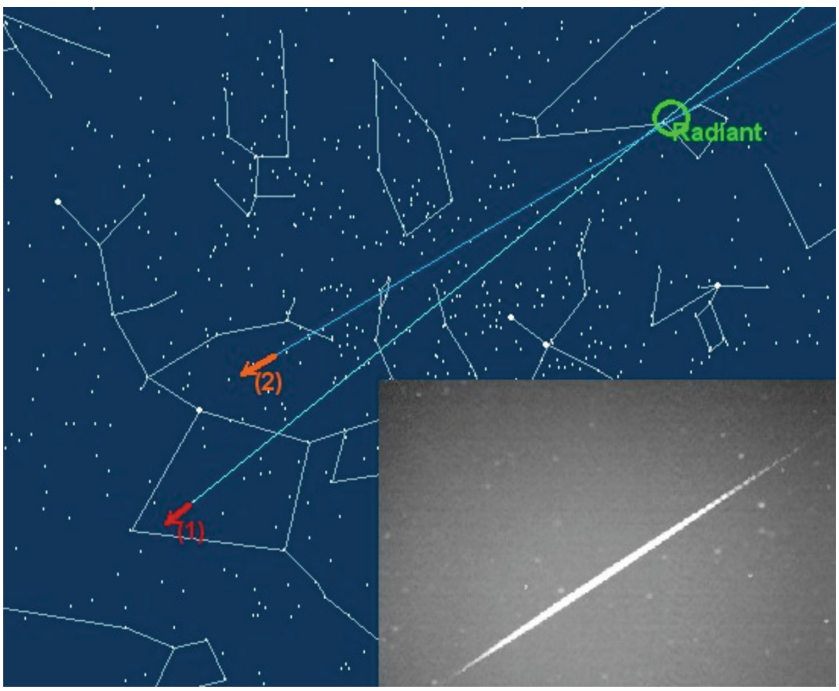

Figure 1. Accurate astrometric measurements of Giacobinid meteors in reference with background stars allow us to infer their respective radiants. On the bottom-left border a −2 meteor recorded at 20h54m52s UTC from Seville [2] SPMN station. The stellar chart shows the event from two stations and its apparent radiant derivation.

involved in the process, see e.g. Williams 2002, or a shorter version in Williams 2004). However, such spreading takes time and meteoroids ejected from the parent in the last few hundred years will still be preferentially clumped close to the comet location on its orbit. Meteor storms can thus be expected when the stream is young at the time where the comet is close to perihelion (see Williams 1997 for a discussion of this process). The appearance of a storm however depends both on how close the nodal distance of the stream orbit is to the Sun–Earth distance and on how short the time interval is between the meteoroid clump passing through the node and the Earth reaching the same point as was shown by Wu & Williams (1995, 1996). This principle was also used by Asher (1999) to explain the Leonid storms.

Comet 21P/Giacobini–Zinner is one comet that is capable of producing a dense meteoroid stream which can result in a fantastic meteor display when the Earth passes through the centre of the stream close. Such storms were seen in 1933 and 1946 as the Draconid meteor storms (also historically called the Giacobinids) when rates went up to ZHR = 10 000 (Jenniskens 2006). Such meteor displays are among the strongest storms ever seen. The circumstances both in terms of nodal distance and time between the comet being at its node and the Earth passing this point were predicted to be similar again in 2011 (Jenniskens 2006; Maslov 2011; Vaubaillon et al. 2011). All the models predicted that on 2011 October 8.7 the Earth would encounter the dust trails left by comet 21P/Giacobini–Zinner during its 19th and 20th century perihelion approaches.

It is important to remember that the spatial density of meteoroids in streams can decrease with time. Both planetary perturbations due to close encounters with planets (Hughes, Williams & Fox 1981; Jenniskens 1998) and mutual collisions among particles from the same or different dust trails can contribute to remove meteoroids from the stream (Babadzhanov et al. 1991; Williams et al 1993; Jenniskens 1998). Collisions with Zodiacal dust particles can also cause vaporization or fragmentation (Trigo-Rodríguez et al. 2005). Hence, even if the encounter circumstances are identical, the above effect can reduce the observed strength of a storm.

The 21P dust trails were obviously older in 2011 than in either 1933 or 1946 and so were expected to be less dense. The decreased flux number density expected for the comet trails was confirmed as during the 2011 Draconid shower the ZHR was less than 1000, making it technically an outburst rather than a storm. The storm was also not so visible to the general public, because of the previously noted presence of the Moon (Jenniskens 2006; Badzhanov, Williams & Kokhirova 2008). However, modern recording systems can work well even in non-favourable conditions, and so a special observing campaign was initiated for the 2011 Draconids. For this, a multistation CCD and video monitoring systems of the Spanish Meteor Network (SPMN) were used. An additional amateur campaign was also initiated. The SPMN high-sensitivity CCD allowed reliable flux and orbital information on the meteoroids that produced the outburst to be obtained. In addition, a -10.5 ± 0.5 absolute magnitude Draconid bolide over Andalusia, Spain was observed implying that the original meteoroid had a mass of about 13 kg (Madiedo et al. 2013). Large fireballs also produced long-lasting persistent trains, and some examples of such spectacular phenomena are given.

This paper has three main goals. First, to summarize the results on the meteoroid flux at the Earth from 21P dust trails derived from visual, video and radio stations during 2011 October. Secondly, to present the trajectory, radiant and orbital data of the most precise orbits computed so far by the SPMN. Thirdly, to compare observational data with the theoretical forecasting in order to provide information on the small-scale structure of the 21P dust trails. This information will be of use for future forecasting of Earth's encounters with cometary dust trails, particularly to better quantify the effects of aging processes in meteoroid streams.

2 INSTRUMENTATION, DATA REDUCTION AND OBSERVATION SITES

Trigo-Rodríguez et al. (2004a,b) have already outlined the first steps in the development of the SPMN that use low-scan-rate all-sky CCD cameras with +2/+3 meteor Lm. In 2006, a further expansion of the network took place when two new all-sky CCD stations in Catalonia and three video stations in Andalusia were added. There are now 25 stations distributed all over Spain, from which the considered for this work are listed in Table 1. The main goal of the monitoring project is to increase the observations of meteor and fireball activity from multiple stations (Trigo-Rodríguez et al. 2006, 2007). The SPMN stations use high-sensitivity CCD and video cameras to monitor the night sky. The video cameras are equipped with a 1/2 arcsec Sony interline transfer CCD image sensor with their minimum lux rating ranging from 0.01 to 0.0001 lx at f1.4 (Madiedo & Trigo-Rodríguez 2007). Aspherical fast lenses with focal length ranging from 4 mm (fisheye) to 25 mm and focal ratio between 1.2 and 0.8 are used for the imaging objective lens that typically reach a Lm of +4. In this way, different areas of the sky can be covered by every camera and point-like star images are obtained across the entire field of view. The observing stations are automatically switched on and off at sunset and sunrise, respectively. The cameras generate video imagery at 25 frames s^{-1} with a resolution of 720×576 pixels^2 and are continuously sent to PC computers through a video capture card. Computers execute software (UFOCAPTURE, by SonotaCo) for automatic detection of meteors and storage of the corresponding frames on hard disc. Since the time of a meteor appearance is crucial in orbital determination, the computers are synchronized by means of Global Positioning System (GPS) devices. In this way, the time is measured with an accuracy of 10^{-1} s along the entire meteor path.

Astrometric reduction of imagery is performed using software described elsewhere (Trigo-Rodríguez et al. 2002, 2004a; Madiedo, Trigo-Rodríguez & Lyytinen 2011). In any meteor event, the software obtains a composite image where automatic detection of stars is achieved. The stars are then measured one at a time and those with significant signal-to-noise ratios are selected for astrometric reduction. Note that no software is used for automatic astrometry of the images so that the observer performs the precise astrometry for stars in the composite image and for the meteor moving in each individual frame. It is then necessary to identify meteors that are common to several observing stations. Under normal meteor activity circumstances, a preliminary search through the data base of meteors that appeared during the same observing interval produces the unequivocal identification of common multiple-station meteors if GPS time calibration is performed in all stations. An interesting application in our software packages is particularly useful for meteor storms, namely the ability to predict the position of every meteor from each station once the astrometry from one station is completed and assuming the typical values of ablation height. The astrometric measurements from each station are then introduced into our NETWORK and AMALTHEA software packages (Trigo-Rodríguez et al. 2003; Madiedo et al. 2011), which compute the equatorial coordinates of the meteors with an astrometric accuracy of about $0\overset{\circ}{.}01$ and also determine the apparent and geocentric radiant of common meteors. Once identified, from the measured sequences recorded in

Table 1. SPMN stations involved in the Giacobinid high-resolution campaign. Acronyms for the different imaging systems are: AS (low-scan-rate CCD all-sky camera), WF (low-scan-rate CCD wide-field camera) and WFV (wide-field video cameras).

Station	Station (Province)	Longitude	Latitude (N)	Alt. (m)	Imaging system
1	Montsec, OAdM (Lleida)	00° 43′ 46″ E	42° 03′ 05″	1570	AS
2	Montseny (Girona)	02° 31′ 14″ E	41° 43′ 17″	300	WFV
3	Folgueroles (Barcelona)	02° 19′ 33″ E	41° 56′ 31″	580	WFV
4	Seville (Seville)	05° 58′ 50″ W	37° 20′ 46″	28	WFV
5	Cerro Negro (Seville)	06° 19′ 35″ W	37° 40′ 19″	470	WFV
6	El Arenosillo (Huelva)	07° 00′ 00″ W	36° 55′ 00″	30	AS+WFV
7	El Picacho (Cádiz)	05° 39′ 01″ W	36° 31′ 19″	392	WFC
8	Madrid-UCM (Madrid)	03° 43′ 34″ W	40° 27′ 03″	640	WFC
9	Villaverde del Ducado (Guadalajara)	02° 29′ 29″ W	41° 00′ 04″	1,100	WFC
10	Toledo	03° 57′ 29″ W	39° 49′ 30″	639	WFC
11	Sierra Nevada (Granada)	03° 23′ 05″ W	37° 03′ 51″	2896	WFC
12	La Hita (Toledo)	03° 10′ 59″ W	39° 34′ 05″	674	WFC

Table 2. Magnitude distribution of Draconids on 2011 October 8 and 9.

Method	Number	−4	−3	−2	0	+1	+2	+3	+4	+5	r
Visual	396	4	5	12	34	70	97	123	48	3	2.3 ± 0.2
Video	75	1	2	3	6	13	20	27	3	–	–

two or more stations, the software estimates by triangulation of the atmospheric trajectory and radiant for each meteor.

It is important to explain and quantify the errors in the results. The accuracy of the astrometric data is directly measured from the standard deviation of the background stars compared with the meteor positions as explained in Trigo-Rodríguez et al. (2003). From the inferred beginning and ending meteor coordinates from both stations, and their respective standard deviation uncertainties the radiant location is obtained. Then the astrometric accuracy propagates into a standard deviation in the radiant position for each meteor as given in Table 5. We selected favourable cases for astrometric reduction, except when the fields of view are wide and slightly distorted due to spherical aberration. Even when correction of that effect has been implemented following the approach by Steyaert (1990), instrumental scattering is still notable in the radiant data as shown in Fig. 3. We suspect that this effect could be due to the pixel size of the detector in which the meteor image is focused and becomes larger as the distance between the meteor and the apparent radiant increases, so the best way to deal with it is probably measuring a large number of meteors to attenuate statistically the scattering. In fact, the averaged geocentric radiant fits well the expected theoretical position as is explained in the discussion.

Finally, in order to determine orbital elements from our trajectory data we used the AMALTHEA program that provides reliable trajectory, physical properties and orbital data.

3 OBSERVATIONAL RESULTS: SPATIAL FLUXES, TRAJECTORY, RADIANT AND ORBITAL DATA

3.1 Determination of population index and meteoroid spatial fluxes

Because they provide photon counts for every pixel, CCD cameras allow a very accurate determination of stellar and meteor magnitudes to be made. In all-sky CCD imaging a simplistic approach is adopted whereby meteor magnitudes are derived by comparing the intensity level of the pixels near the maximum luminosity of the meteor trail with those of nearby stars. The different angular velocity of the meteors should be taken into account as a function of the distance to the radiant and the typical duration of flares, but in general for meteors a difference of four magnitudes is produced, i.e. a meteor of magnitude −2 exhibits a path with similar intensity to a star of magnitude +2. General formulae to take into account the different angular velocity of the sources (stars and meteors) were compiled by Rendtel (1993). This generalization is not valid for meteors that appear below 30° of altitude since they need to be additionally corrected for atmospheric extinction losses, that we also corrected. Our measured magnitudes were additionally tested for correctness to within ±0.5 mag by performing simultaneous visual observations and correlating the meteor peak to the imaging record.

From the visual and video derived meteor magnitudes, the magnitude distribution for the nights of 2011 October 8 and 9 was obtained and is given in Table 2. From this a population index for the three experienced visual observers of $r = 2.3 \pm 0.3$ ($N = 393$) was derived. This value was used to estimate the visual ZHR as well as to convert to the spatial flux of meteoroids the meteors brighter than +6.5 km^{-2} given in Table 3. The results suggest that at least two peaks with a maximum visual (human) rate are close to ZHR = 400. In general, the values confirm the visual rates compiled by amateurs in the framework of the International Meteor Organization (IMO web page). A general discussion of the results presented in Tables 3 and 4 is particularly useful to understand the interception of 21P dust trails by Earth. Observations can be compared with the excellent forecast of the interception of the 21P dust trail by Earth made in table 3 of Vaubaillon et al. (2011). The determined flux in the $]-\infty, +5]$ magnitude range was maximum at solar longitude 195.°0106 (2011 October 8 at ∼19h38m UTC) when the flux reached $(113 \pm 16) \times 10^{-3}$ km^{-2} h^{-1}. This peak fits perfectly, particularly taking into account the arbitrary periods taken, with the time forecast for the 1907 dust trail at solar longitude 195.°0059 (Vaubaillon et al. 2011). A second peak occurs at solar longitude 195.°0311 (2011 October 8 at ∼20h08m UTC) when the visual flux reached

Table 3. ZHR and flux estimations.

Interval (UT)	λ_o (°)	Number of meteors	ZHR	ε	Flux ($\times 10^{-3}$ km^{-2} h^{-1})	$\varepsilon_{\rm flux}$	r	ε_r
19h00–19h15	194.990 13	12	127	37	34	10	3.2	0.6
19h15–19h30	195.000 38	33	223	39	60	10	2.1	0.5
19h30–19h45	195.010 63	51	419	59	113	16	2.3	0.7
19h45–20h00	195.020 88	42	259	40	70	11	2.0	0.7
20h00–20h15	195.031 13	63	371	47	100	13	1.8	0.6
20h15–20h30	195.041 38	39	235	38	64	10	1.9	1.2
20h30–20h45	195.051 63	21	230	54	62	15	3.5	1.2
20h45–21h00	195.061 88	30	269	49	73	13	2.7	0.8
21h00–21h15	195.072 13	45	394	59	106	16	2.1	0.7
21h15–21h30	195.082 38	24	220	45	59	12	2.0	1.2
21h30–22h00	195.097 75	12	50	14	14	4	2.0	1.4
22h00–22h30	195.118 25	21	129	28	35	8	2.4	1.7

Table 4. Backscatter radio counts obtained by Diego Rodríguez in the observing interval discussed here. In bold are the high rates that reveal dust trail crossing discussed in the text.

Interval (UT)	Counts	Interval (UT)	Counts	Interval (UT)	Counts	Interval (UT)	Counts	Interval (UT)	Counts
14:10–14:20	4	17:10	11	20:10	**39**	23:10	3	2:10	1
14:20	2	17:20	6	20:20	22	23:20	4	2:20	2
14:30	2	17:30	5	20:30	21	23:30	6	2:30	4
14:40	2	17:40	**14**	20:40	11	23:40	4	2:40	3
14:50	5	17:50	**6**	20:50	**16**	23:50	2	2:50	2
15:00	1	18:00	**11**	21:00	**19**	0:00	4	3:00	3
15:10	6	18:10	9	21:10	**15**	0:10	0	3:10	4
15:20	4	18:20	4	21:20	5	0:20	5	3:20	0
15:30	2	18:30	6	21:30	9	0:30	7	3:30	6
15:40	7	18:40	9	21:40	15	0:40	8	3:40	1
15:50	2	18:50	5	21:50	9	0:50	5	3:50	8
16:00	2	19:00	19	22:00	5	1:00	1	4:00	4
16:10	3	19:10	11	22:10	12	1:10	5	4:10	3
16:20	3	19:20	13	22:20	6	1:20	6	4:20	5
16:30	6	19:30	**29**	22:30	7	1:30	5	4:30	5
16:40	7	19:40	**25**	22:40	6	1:40	4	4:40	5
16:50	7	19:50	20	22:50	3	1:50	2	4:50	6
17:00	3	20:00	**26**	23:00	0	2:00	5	5:00–5:10	2

$(102 \pm 13) \times 10^{-3}$ km^{-2} h^{-1}. This second peak also agrees with that forecasted by Vaubaillon et al. (2011) for the dust trail released by comet 21P during the 1900 perihelion passage. Finally, a third peak of similar intensity occurred at solar longitude 195°.0721 (2011 October 8 at ∼21h08m UTC) when the visual flux reached $(106 \pm 16) \times 10^{-3}$ km^{-2} h^{-1}. That peak also produced bright meteors, and may be the result of several older dust trail components as it is not clearly predicted in Vaubaillon et al. (2011). The visual comparison among visual and video data shows that the third peak was not recorded in video observations (Fig. 2a). Despite this, a moderate peak at that solar longitude is seen in IMO data (IMO web page), but the absence in our video records perhaps supports the idea that this peak was mainly composed of faint meteors as suggested by the decreasing population index values (see Fig. 2b). The existence of this was confirmed by backscatter radio observations (see radio counts in Table 4) with three consecutive 10 min intervals exhibiting high rates around 21h00m UTC. A discone antenna was used together with a Yaesu VR5000 receiver working at 143.05 MHz from Guadarrama Observatory (Madrid). This radio data seem to reveal more moderate radio bursts at 17h15m and 17h45m UTC probably associated with the 1887 dust trail, and another one at 19h05m that could be tentatively associated with the 1894 dust trail (table 3 of Vaubaillon et al. 2011). The Giacobinid flux was about one order of magnitude lower for bright meteors recorded by video cameras with +3 Lm that night. Consistently, the corrected SPMN counts were found to be 40 times stronger during the outburst than for sporadic rates that usually reach ∼10 meteors h^{-1}.

To roughly compute the amount of mass delivered by comet 21P to Earth during the 2011 outburst ($M_{\rm DEL}$) we use a first order of magnitude approach. $M_{\rm DEL}$ is computed by considering the number of meteoroids in each magnitude range and multiplying them by the meteoroid mass given in appendix C, equation C.12 of Jenniskens (2006). The number of meteoroids in each magnitude range is fitted to be what is required to produce an averaged global ZHR of ∼400 with a population index: $r \sim 2$ (Table 3). As the ZHR was slightly lower than that in most intervals, our computation is an upper limit for the mass delivered. According to the radio data shown in Table 4, the outburst level was sustained for about 6 h, and that value was used for the final computation. The equations that describe the procedure are

$$M_{\rm DEL} = \sum_{i}^{+6} m_i \times N_i \quad \text{where} \quad \sum_{i}^{+6} N_i = \mathrm{ZHR}(r)_{\rm observed}.$$

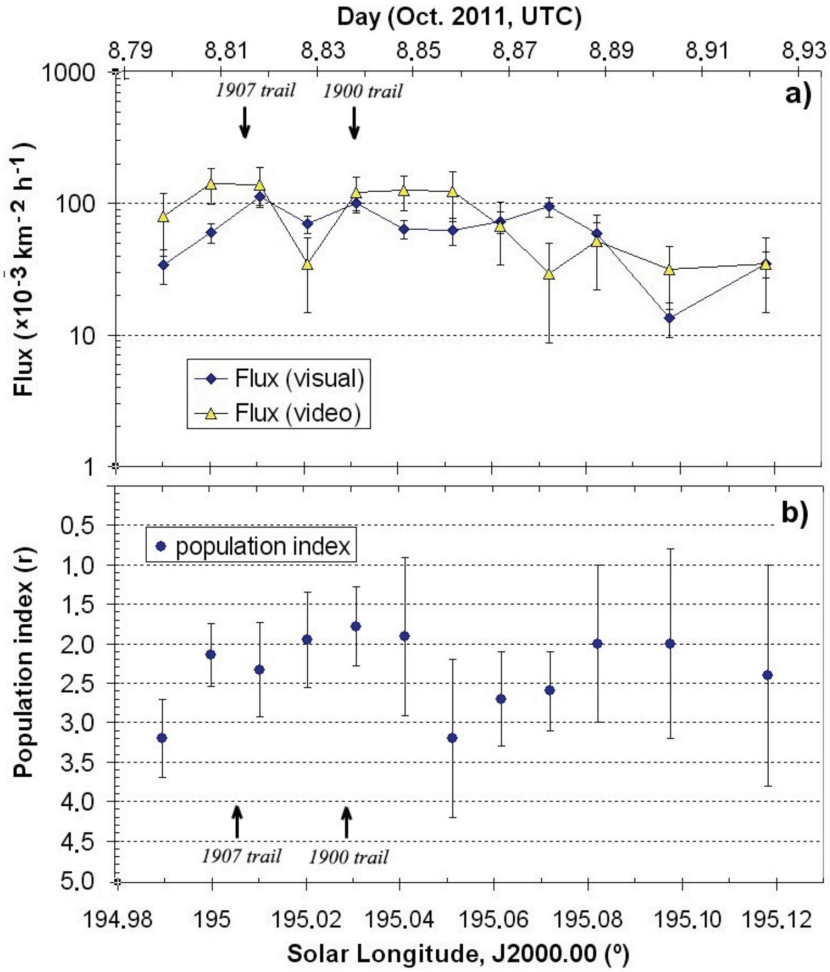

Figure 2. (a) Derived meteoroid fluxes and (b) population index values for visual and video data.

This gives the meteoroid mass delivered into a subtended atmospheric volume seen by a visual observer (see Koschack & Rendtel 1990a,b). This mass needs to be multiplied by a factor to cover the total mass reaching all Earth. The final result of such calculations yields $M_{\rm DEL} = 950 \pm 150$ kg delivered during the 6 h of outburst. To obtain the mass uncertainty we applied the common law of propagation of errors having into account the uncertainty in the meteor flux and the population index. Obviously, a significant part of this mass was ablated during atmospheric interaction, but the rest contributed significantly to the release of elements in the upper atmosphere.

3.2 Trajectory, dynamic strength and radiant data

The observed common field for the stations was initially programmed (Section 2) so that double-station meteors were required to have convergence angles greater than 20° to allow accurate determination of trajectory and geocentric radiant. The convergence angle (Q) is the angle between the two planes delimited by the observing sites and the meteor path in the triangulation. The trajectory data of 16 accurately reduced meteors are given in Table 5, which shows the SPMN code used for identification, the apparent visual magnitude ($M_{\rm v}$), the meteor trail beginning and end height on the Earth's surface ($H_{\rm b}$ and $H_{\rm e}$ in km), the geocentric radiant coordinates ($\alpha_{\rm g}$ and $\delta_{\rm g}$ to Equinox 2000.00) and the velocity in km s^{-1} (at the top of atmosphere, geocentric and heliocentric). The velocity at the top of the atmosphere was measured in the upper parts of the luminous trajectories, and we double checked that the measured values adjust to the values derived for the following frames.

From the 16 Draconid radiants we obtained an averaged geocentric radiant at $\alpha = 263.0 \pm 0.^{\circ}4$ and $\delta = +55.3 \pm 0.^{\circ}3$. For comparison, the theoretical radiants given by Maslov (2011) or Jenniskens & Vaubaillon (2011) are compiled in Table 6. The orbital parameters are given in Table 7. The radiant and average velocity data based on the data in Table 5 are in close agreement, but far more precise, than those discussed in the IMO list by Langbroek (2011) from a joint American/German/Dutch video campaign to study the outburst (last row in Table 6). Finally, in Fig. 3 are shown the October Draconid geocentric radiants compared with the theoretical position given by Maslov (2011).

3.3 Orbital elements of 2011 October Draconid meteors

From the radiant position, appearance time and velocities estimated for the Draconid meteors listed in Table 5 we derived the orbital elements shown in Table 7. Due to the high meteor rate, we decided to name the meteors from the appearance time (SPMN: hour:minute:second). This way is also useful to identify the probable dust trails to which the meteors or fireballs belong. For example, the first eight meteors in Table 7 appeared in 1 h interval from 8.78

Table 5. Trajectory, radiant and velocity data for the 16 high-precision Draconids reduced so far. Equinox (2000.0).

SPMN code	M_v	H_b	H_{max}	H_e	α_g (°)	δ_g (°)	V_∞	V_g	V_h
183440	−1	95.2	90.3	87.7	263.7 ± 0.3	55.3 ± 0.3	23.6 ± 0.3	20.95	38.94
184038	−2	95.7	90.5	87.1	263.48 ± 0.14	55.55 ± 0.16	23.4	20.74	38.88
185050	−5	96.4	85.3	81.7	266.9 ± 0.4	58.2 ± 0.4	24.5	21.94	39.27
185948	−3	102.3	92.7	85.6	263.6 ± 0.3	55.9 ± 0.3	23.8	21.18	39.18
191104	−4	96.7	87.6	78.6	262.7 ± 0.3	55.6 ± 0.3	23.8	21.18	39.12
191929	−2	97.9	92.3	88.5	262.65 ± 0.14	55.57 ± 0.14	23.5	20.88	39.11
192250	−6	98.5	93.7	89.5	258.9 ± 0.4	54.2 ± 0.4	22.9	20.19	38.67
192840	−1	94.3	84.2	83.6	263.6 ± 0.3	54.5 ± 0.3	23.2	20.5	39.1
194759	−11	107.3	99.1	77.1	264.15 ± 0.14	54.69 ± 0.14	23.3	20.68	39.02
195157	−4	95.4	92.3	88.5	258.19 ± 0.11	55.15 ± 0.14	23.2	20.57	38.71
201354	−4	93.9	89.5	85.2	268.9 ± 0.4	55.81 ± 0.06	23.0	20.32	38.93
201440	−3	103.7	98.4	93.1	261.14 ± 0.14	55.87 ± 0.08	23.2	20.55	38.86
201453	−2	91.4	89.1	87.4	268.90 ± 0.18	56.49 ± 0.05	23.0	20.29	38.73
201849	−4	92.1	88.9	82.6	259.6 ± 0.5	53.58 ± 0.14	22.9	20.22	38.83
203103	−3	92.8	87.5	86.8	263.2 ± 0.4	55.30 ± 0.03	23.6	21.03	38.18
204801	−4	104.1	85.9	81.4	257.6 ± 0.3	54.9 ± 0.3	23.5	20.91	38.87
Average	–	97.7	90.5	85.1	263.0 ± 0.4	55.3 ± 0.3	23.4	20.76	38.90

Table 6. Predicted radiant positions and averaged geocentric velocity (V_g) of members of 21P dust trails according to Maslov (2011), Vaubaillon et al. (2011) and Jenniskens & Vaubaillon (2011). Equinox (2000.00).

Trail/source	RA (°)	Dec. (°)	V_g (km s^{-1})	Source
1900	263.3	+55.8	20.9	Maslov (2011)
1873–1894	263.3	+55.4	–	Jenniskens & Vaubaillon (2011)
SPMN	263.0 ± 0.4	55.3 ± 0.3	20.76	This work (Table 5)
AGD campaign	262.8 ± 0.7	+55.5 ± 1.1	20.98 ± 0.95	Langbroek (2011)

Table 7. Orbital elements of the 16 Giacobinid meteors. Equinox (2000.00).

SPMN code	Day	q (au)	a (au)	e	i (°)	ω (°)	Ω (°)
183440	8.774 079 86	0.996 88 ± 0.000 18	3.42 ± 0.25	0.709 ± 0.021	31.9 ± 0.4	185.98 ± 0.24	194.973 17
184038	8.778 217 59	0.996 01 ± 0.000 08	3.53 ± 0.17	0.718 ± 0.013	31.3 ± 0.3	172.98 ± 0.11	194.977 27
185050	8.785 303 24	0.998 43 ± 0.000 13	3.80 ± 0.25	0.737 ± 0.017	33.5 ± 0.3	176.8 ± 0.3	194.984 22
185948	8.791 528 94	0.996 71 ± 0.000 19	3.7 ± 0.3	0.729 ± 0.022	32.1 ± 0.4	186.14 ± 0.24	194.990 40
191104	8.799 347 22	0.996 84 ± 0.000 18	3.6 ± 0.3	0.724 ± 0.022	32.2 ± 0.4	185.99 ± 0.11	194.998 11
191929	8.805 204 86	0.995 50 ± 0.000 10	3.6 ± 0.3	0.72 ± 0.03	31.5 ± 0.4	172.46 ± 0.14	195.0039
192250	8.807 525 46	0.9928 ± 0.0004	3.2 ± 0.3	0.69 ± 0.03	30.6 ± 0.5	169.9 ± 0.4	195.006 23
192840	8.811 574 07	0.9964 ± 0.0002	3.6 ± 0.2	0.72 ± 0.02	30.8 ± 0.3	173.4 ± 0.2	195.0102
194759	8.824 988 43	0.996 72 ± 0.000 07	3.7 ± 0.3	0.731 ± 0.021	31.1 ± 0.4	186.12 ± 0.13	195.023 46
195157	8.827 747 69	0.991 90 ± 0.000 17	3.20 ± 0.22	0.692 ± 0.020	31.2 ± 0.6	169.21 ± 0.19	195.026 10
201354	8.842 994 21	0.9987 ± 0.000 15	3.41 ± 0.23	0.71 ± 0.03	30.8 ± 0.3	177.5 ± 0.3	195.041 25
201440	8.843 519 68	0.995 19 ± 0.000 11	3.21 ± 0.19	0.684 ± 0.020	31.2 ± 0.3	172.02 ± 0.21	195.041 74
201453	8.843 673 61	0.9988 ± 0.0003	3.22 ± 0.21	0.690 ± 0.020	31.0 ± 0.6	177.71 ± 0.11	195.0418
201849	8.846 400 46	0.9931 ± 0.0003	3.3 ± 0.3	0.700 ± 0.021	30.5 ± 0.3	170.2 ± 0.4	195.0446
203103	8.854 900 46	0.9900 ± 0.0005	2.79 ± 0.15	0.645 ± 0.019	32.8 ± 0.4	167.6 ± 0.4	195.0529
204801	8.866 672 45	0.9917 ± 0.0003	3.34 ± 0.24	0.704 ± 0.021	31.7 ± 0.4	169.2 ± 0.3	195.064 59
Average	–	0.9954 ± 0.0003	3.40 ± 0.23	0.705 ± 0.021	31.5 ± 0.4	174.86 ± 0.23	–

to 8.81 October 2011. Consequently, looking at Fig. 2(a), they are very likely associated with the 1907 dust trail. The 1900 dust trail detections start with the extraordinary −10.5 mag bolide SPMN 194759 shown in Fig. 4 (see detailed study about its emission spectrum by Madiedo et al. 2013). At that interval from 8.82 to 8.87 October we computed high-resolution orbits of eight bright meteors, six of them practically in the fireball range. This would suggest that a small fragmentation event could have taken place on 21P during its 1907 perihelion passage since it is not possible for meteoroids larger than about 10 cm to be ejected by the normal Whipple mechanism (Williams 2004).

4 DISCUSSION

An important consequence of being able to obtain accurate trajectory data is that the physical properties of the meteoroid can be determined. Meteors that exhibited a catastrophic disintegration at the end of their paths allow their dynamic strengths to be determined (Trigo-Rodríguez & Llorca 2006, 2007). This was the case for many of the Draconid meteors. To do this, the aerodynamic strength (S) is required and we have used the equation given by Bronshten (1981):

$$S = \rho_{atm} \times v^2, \quad (1)$$

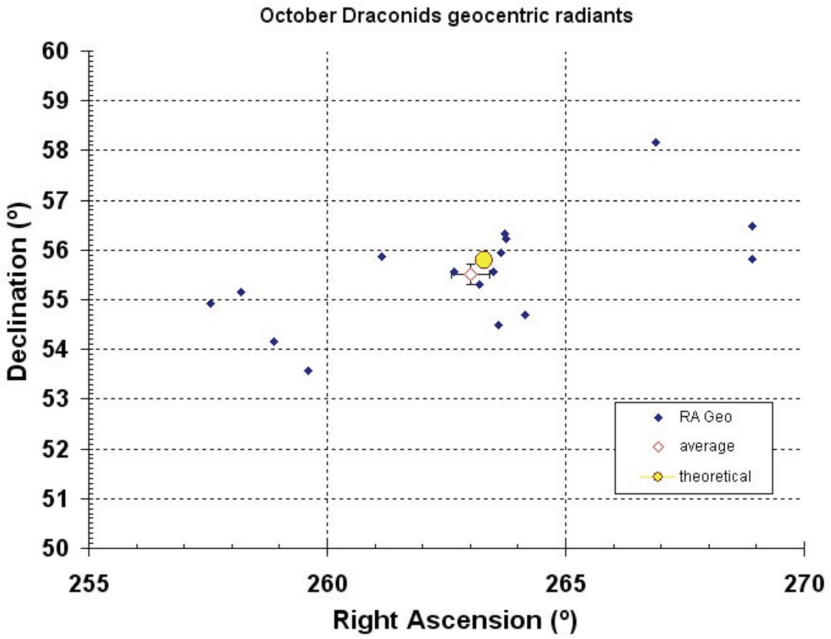

Figure 3. Computed Giacobinid geocentric radiants and our averaged radiant position compared with the theoretical position given by Maslov (2011).

Figure 4. Image sequence taken by Antonio Francisco Marín of an almost stationary −10.5 mag SPMN 194759 bolide seen from El Picacho (Cádiz) and its persistent train left behind. Propagation is nicely seen in the 30 s exposure consecutive images. First picture taken at 19h47m50s UTC, and readout time between images of about 3 s.

where $\rho_{\rm atm}$ is the atmospheric density at the height where the meteoroid breaks up and v is the velocity of the particle at this point to estimate this. If the density is given in kg m^{-3} and the velocity in m s^{-1}, the strength is given in dyne cm^{-2}. Verniani (1969) and Wetherill & ReVelle (1982) applied this equation for determining mechanical stresses. Verniani (1969) pointed out those meteoroids following typical cometary orbits fragment when the pressure exceeds 2×10^4 dyn cm^{-2}.

Table 8. Disruption heights. Velocity at disruption point. Atmospheric US standard density from which the dynamic strengths of selected Draconids are computed.

SPMN code	Magnitude	H_{max} (km)	v (km s^{-1})	ρ ($\times 10^{-9}$ g cm^{-3})	τ ($\times 10^{2}$ dyn cm^{-2})
185050	−5	85.3	20.1	6.3528	35 ± 1
191104	−4	87.6	20.4	4.1700	25 ± 1
194759	−11	99.1	22.5	0.3855	1.9 ± 0.1
204801	−4	85.9	21.2	5.7007	35 ± 1

In Table 8, we show the heights, velocities and dynamics strengths for four Draconids. Three of them exhibited catastrophic disruptions so we computed the strength for those points, but in the case of the bright bolide SPMN 194759 the strength was computed in the first major flare (as discussed in Madiedo et al. 2013). We have computed the dynamic strength for these three cases following the approach described in Trigo-Rodríguez & Llorca 2006, Trigo-Rodríguez & Llorca 2007. The Draconids appear to be the most fragile meteoroids from all the cometary showers with typical dynamic strengths below $\sim 10^3$ dyn cm^{-2}.

These results are consistent with the low strength cometary populations identified by Jacchia (1958) and Ceplecha (1958). On the other hand, Verniani (1969, 1973) and Millman (1972) found that most of the sporadic meteoroids of cometary origin are highly porous. In fact, cometary disruption events are occurring even at large heliocentric distances, characteristic of extremely crumbly structures (Sekanina 1982). Such events provide clues to the extremely low tensile strengths of cometary nuclei, estimated to be between several times 10^3 and 10^5 dyn cm^{-2} (Donn 1963). These measured strengths are consistent with the behaviour of cometary meteoroids that typically fragment in the upper atmosphere at similar aerodynamic pressures. Further clues about the nature of cometary meteoroids can be obtained from the study of ballistic aggregation experiments (Krause & Blum 2004). All these data suggest that cometary meteoroids may be fractal aggregates with extremely high porosity.

The study of the atmospheric interaction of cometary meteoroids penetrating the atmosphere at low geocentric velocities is also interesting from a cosmochemical point of view. From the changes in the population index and in the number of fireballs since these trails were crossed by Earth in the 1930s, we have evidence that Draconid meteoroids are being progressively eroded. The occurrence of such a progressive process, which occurs in the interplanetary medium may be explained in the context of the recent discovery of ultracarbonaceous micrometeorites in Antarctica (Duprat et al. 2010). Such fragile materials belong to some primitive parent bodies of isotopic and chemically exotic nature. For example, they exhibit high D/H ratios, abundant organic matter and μm-sized or smaller silicate particles similar to these found in porous interplanetary dust particles (IDPs). The delivery of biogenic elements by encounters with dense cometary trails along the eons probably has been relevant. Blum et al. (2006) reasoned from accretionary, dynamic and evolutionary arguments that hundred- to kilometre-sized primitive asteroids and comets should exhibit a fragile nature: extremely low bulk density and high porosity. Recent Stardust collection of cometary dust in the coma of pristine comet 81P/Wild 2 also provided interesting clues on the nature of these materials (Brownlee et al. 2006; Trigo-Rodríguez et al. 2008). They are aggregates whose structure is similar to carbonaceous IDPs or primitive carbonaceous chondrites. Consequently, we expect a 21P/Giacobini–Zinner cometary meteoroid structure composed of a matrix rich in C and other biogenic elements, and additional chondrules, and tiny and rarer refractory inclusions. Due to the relative low bulk density and large porosity of those aggregates, the tensile strength of 21P/Giacobini–Zinner meteoroids is much lower than for any known terrestrial mud or sandstone. This fragile nature explains the brilliant catastrophic disruptions that we typically observe in the upper atmosphere for cometary origin bolides (Trigo-Rodríguez et al. 2007, 2009; Trigo-Rodríguez & Blum 2009). In fact, about 20 per cent of the large fireballs recorded by the Prairie Network ended up in a sudden overwhelming fragmentation that translates into a flare, and about 60 per cent of the cases experienced one or several fragmentations along their path (Ceplecha et al. 1998). This occurs when the meteoroid feels an increasing dynamic pressure ($p = \rho \times v^2$) as it penetrates the atmosphere. When the loading pressure surpasses the material strength required for fragmentation the body breaks apart and, as a consequence of the flight and shock wave shaking, disruption is imminent. Once disrupted, most of the fine-grained material exposed to the frontal bowl shock is very efficiently vaporized, as meteor spectroscopy reveals that the material quickly reaches temperatures well over the sublimation point of silicates (Borovička 1993, 1994; Trigo-Rodríguez et al. 2003; Madiedo et al. 2013). On the basis of fireball spectroscopy, it is suspected that catastrophic disruptions can disperse dust back and far from the shock wave frontal region where bolide experiences higher temperatures (Trigo-Rodríguez & Martín-Torres 2013). Ablation temperature is lower for low-entry velocity meteoroids, and particularly in these cases the exposure of the released materials to heat may not be identical. A catastrophic break-up could move dust laterally and generate turbulence. If so, there is room for a small percentage of the body to survive, as supported by the discovery of unmelted dust and small micrometeorite fragments that are slowly setting down towards the surface (Taylor, Lever & Harvey 2000; Genge 2008; Duprat et al. 2010). Indirect evidence on the survival of small quantities of dust in meteor spectroscopy could be the presence of a continuum of radiation in meteor spectra, or the persistent trains observed for seconds or even minutes after the extinction of the fireball phase. In any case, meteoroid smokes produced by recondensation of vaporized minerals can also contribute, and the association needs to wait until achieving spectroscopy of much higher resolution and fast video cameras. In any case, proof that dust can survive was provided in high-resolution spectra obtained during the re-entry and ablation of the impact plumes produced on the Jovian atmosphere as a consequence of the impact of comet Shoemaker-Levy 9 in 1994 July at a velocity of 60 km s^{-1} (Fitzsimmons et al. 1996). These authors found that most of the light emission came from silicate grains ablated in the different phases, even in the case of a bolide produced by tens of metre-sized cometary fragments. On the other hand, fireball entry models not only can predict survival of silicate dust, but also of more friable compounds e.g. organics in the internal

structure. In this sense, Blank et al. (2001) have shown that asteroids and comets impacting the atmosphere of Earth are delivering small amounts of complex organics if the impact geometry and velocity are favourable to produce a moderate deceleration and setting of the materials in the atmosphere.

Another important aspect to consider is the thermal processing that affects the materials subjected to ablation in the fireball column. As a consequence of the heat associated with the collisions of atmospheric gases, meteoric minerals are ablated, vaporized and dissociated. Elemental lines and molecular bands are remarkable features in bolide spectra (Fig. 1). It has been demonstrated that most of the fireball chemistry behind radiating light can fit perfectly a thermodynamic equilibrium model (Borovička 1993, 1994; Trigo-Rodríguez et al. 2003). This behaviour is probably a consequence of the quick mixing of air and meteoric plasma promoted by the supersonic movement, meteoroid spinning and subsequent induced turbulence around the bolide. It is important to remark, however, that the production of different gases can be avoided in environments with different chemistry and radiative flux.

5 CONCLUSIONS

Despite the expectation created with the return of 21P/Giacobini–Zinner's dust trails to Earth's vicinity on 2011 October 8, the display was moderate compared to previous encounters. Dust trails left by the comet were precisely forecasted through the perihelion approach, and that achievement was in practice an excellent advantage to set up a special SPMN campaign with smaller fields of view than those used in usual fireball network patrol. The video CCD camera systems whose excellent performances for meteor recording were initially described in Madiedo & Trigo-Rodríguez (2007) are again showing their potential with the current data. In spite of the moderate Draconid activity, our camera systems were able to record hundreds of meteors all over Iberian Peninsula by using high-sensitivity 1/2 arcsec black and white CCD video cameras (Watec, Japan) and 1/3 arcsec progressive-scan sensors attached to modified short-field lenses. We have presented the main results on the orbital and flux data obtained by SPMN camera systems on that night. Unfortunately, the meteor shower did not reach storm category, but the outburst was really remarkable with peaks of activity of several hundreds of meteors per hour. As the meteor activity was predicted in advance special camera systems were set up that were able to cover a wide area network, permitting the collection of very valuable information for optical meteors as faint as magnitude +3. The findings obtained from the 2011 Giacobinid campaign are as follows.

(a) On 2011 October 8 the Earth encountered the dust trails left by comet 21P/Giacobini–Zinner during its 19th and 20th century perihelion approaches. The trails were older than in previous 1933 and 1946 historical encounters, and significantly perturbed by Earth's encounters so they produced an outburst, but not a storm.

(b) Video observations allow the physical behaviour of cometary meteoroids penetrating the atmosphere at low geocentric velocity to be studied. Terminal catastrophic flares are typically produced at dynamic strength pressures over 400 Pa, but for largest meteoroids that can reach about 1 kPa.

(c) SPMN averaged geocentric radiant data in RA $= 263.0 \pm 0.^{\circ}4$ and Dec. $= +55.3 \pm 0.^{\circ}3$ fits the theoretical radiant well inside the astrometric uncertainties.

(d) The above mentioned previous encounters also decreased the meteoroid spatial flux. This is probably a direct consequence of gravitational scattering of the dust trail individual members during such encounters, but it is also probable consequence of a fragile nature of meteors that, having low strength and fractal-like structure, are more exposed to direct collisional erosion (with Zodiacal dust or same-stream meteoroids) and also to solar irradiation. Both space weathering processes are probably decreasing the spatial number density of meteoroids in time-scales of few centuries.

(e) The 2011 Giacobinid flux rates were about one order of magnitude lower than expected. The global mass of 21P cometary materials delivered to Earth was $M_{\rm DEL} = 950 \pm 150$ kg. To improve future models, precise flux determinations as these presented here could be the key to better understand interplanetary space erosive processes, and their direct effect in the diffusion of dust trails and meteor displays.

ACKNOWLEDGEMENTS

We are particularly grateful to all amateur observers that contributed to this study. We acknowledge support from the Spanish Ministry of Science and Innovation (projects AYA2009-13227, AYA2009-14000-C03-01 and AYA2011-26522), Junta de Andalucía (project P09-FQM-4555) and CSIC (grant #201050I043). We also thank the Draconid Recerca en Acció project (granted by Generalitat de Catalunya) in order to promote a cooperative amateur campaign in Catalonia. We also thank Dr Margaret Campell-Brown for many useful suggestions for improving this paper.

REFERENCES

Asher D. J., 1999, MNRAS, 307, 919
Babadzhanov P. B., Wu Z., Williams I. P., Hughes D. W., 1991, MNRAS, 253, 69
Badzhanov P. B., Williams I. P., Kokhirova G. I., 2008, MNRAS, 386, 1436
Blank J., Miller G. H., Ahrens M. J., Winans R. E., 2001, Orig. Life Evol. Biosph., 31, 15
Blum J., Schräpler R., Davidson B. J. R., Trigo-Rodríguez J. M., 2006, ApJ, 652, 1768
Borovička J., 1993, A&A, 279, 627
Borovička J., 1994, Planet. Space Sci., 42, 145
Bronshten V. A., 1981, Physics of Meteoric Phenomena, Geophysics and Astrophysics Monographs. Reidel, Dordrecht
Brownlee D. et al., 2006, Sci, 314, 1711
Ceplecha Z., 1958, Bull. Astron. Inst. Czech., 9, 154
Ceplecha Z., Borovička J., Elford W. G., Revelle D. O., Hawkes R. L., Porubcan V., Simek M., 1998, Space Sci. Rev., 84, 327
Comas Solà J., 1939, in Ramón Sopena, ed., Astronomía. Barcelona, Spain, p. 639
Donn B., 1963, Icarus, 2, 396
Duprat J. et al., 2010, Sci, 328, 742
Fitzsimmons A., Andrews P. J., Catchpole R., Little J. E., Walton N., Williams I. P., 1996, Nat, 379, 801
Genge M., 2008, Earth Moon Planets, 102, 525
Gomes R., Levison H. F., Tsiganis K., Morbidelli A., 2005, Nat, 435, 466
Hughes D. W., Williams I. P., Fox K., 1981, MNRAS, 195, 625
Jacchia L. G., 1958, Smithsonian Contribution to Astrophysics, 2, 181
Jenniskens P., 1998, Earth Planets Space, 50, 555
Jenniskens P., 2006, Meteor Showers and their Parent Comets. Cambridge Univ. Press, Cambridge
Jenniskens P., Vaubaillon J., 2011 Draconids Multi-Instrument Aircraft Campaign (http://draconids.seti.org/)
Koschack R., Rendtel J., 1990a, WGN J. IMO, 18:2, 44
Koschack R., Rendtel J., 1990b, WGN J. IMO, 18:2, 119
Krause M., Blum J., 2004, Phys. Rev. Lett., 93:2, 021103
Langbroek M., 2011, IMO-News Mailing List, Message 2339
Lovell A. C. B., 1954, Meteor Astronomy. Oxford Univ. Press, Oxford

Madiedo J. M., Trigo-Rodríguez J. M., 2007, Earth Moon Planets, 102, 133
Madiedo J. M., Trigo-Rodríguez J. M., Lyytinen E., 2011, Meteoroids: the smallest solar system bodies, 7th Meteoroids Int. Conf., NASA/CP-2011-216469, p. 330
Madiedo J. M., Trigo-Rodríguez J. M., Konovalova N., Williams I. P., Castro-Tirado A. J., Ortiz J. L., Cabrera-Caño J., 2013, MNRAS, doi:10.1093/mnras/stt748
Maslov M., 2011, WGN J. IMO, 39:3, 64
McKinley D. W. R., 1961, Meteor Science and Engineering. McGraw-Hill, New York
Millman P., 1972, in Elvius A., ed., From Plasma to Planet. Wiley, New York, p. 157
Rendtel J., 1993, IMO Monograph 3, Handbook for Photographic Meteor Observations. IMO, Germany
Sekanina Z., 1982, in Wilkening L. L., ed., Comets. University of Arizona Press, Tucson, p. 251
Steyaert C., 1990, Photographic Astrometry. IMO Publ., pp. 61
Taylor S., Lever J. H., Harvey R. P., 2000, Meteorit. Planet. Sci., 35, 651
Trigo-Rodríguez J. M., Blum J., 2009, Planet. Space Sci., 57, 243
Trigo-Rodríguez J. M., Llorca J., 2006, MNRAS, 372, 655
Trigo-Rodríguez J. M., Llorca J., 2007, MNRAS, 375, 415
Trigo-Rodríguez J. M., Martín-Torres F. J., 2013, in Trigo-Rodríguez J. M., Raulin F., Nixon C., Muller C., eds, The Early Evolution of the Atmospheres of the Terrestrial Planets. Springer, New York, in press (ISBN: 978-1-4614-5190-7)
Trigo-Rodríguez J. M., Llorca J., Fabregat J., 2002, Earth, Moon Planets, 91, 107
Trigo-Rodríguez J. M. et al., 2004a, Earth, Moon Planets, 95, 553
Trigo-Rodríguez J. M., Llorca J., Lyytinen E., Ortiz J. L., Sánchez Caso A., Pineda C., Torrell S., 2004b, Icarus, 171, 219
Trigo-Rodríguez J. M., Betlem H., Lyytinen E., 2005, ApJ, 621, 1146
Trigo-Rodríguez J. M., Llorca J., Castro-Tirado A. J., Ortiz J. L., Docobo J. A., Fabregat J., 2006, Astron. & Geophys., 47:6, 26
Trigo-Rodríguez J. M. et al., 2007, MNRAS, 382, 1933
Trigo-Rodríguez J. M., Domínguez G., Burchell M. J., Hörz J Llorca J., 2008, Meteorit. Planet. Sci., 43, 75
Trigo-Rodríguez J. M., Madiedo J. M., Williams I. P., Castro-Tirado A. J., 2009, MNRAS, 392, 367
Vaubaillon J., Watanabe J., Sato M., Horii S., Koten P., 2011, WGN J. IMO, 39:3, 59
Verniani F., 1969, Space Sci. Rev., 10, 230
Verniani F., 1973, J. Geoph. Res., 78, 8429
Wetherill G. W., ReVelle D. O., 1982, in Wilkening L. L., ed., Comets. University of Arizona Press, Tucson, p. 297
Whipple F. L., 1951, ApJ, 113, 464
Williams I. P., 1997, MNRAS, 292, L37
Williams I. P., 2002, in Murad E., Williams I. P., eds, Meteors in the Earth's Atmosphere. Cambridge Univ. Press, Cambridge, p. 13
Williams I. P., 2004, WGN J. IMO, 32:1, 11
Williams I. P., Hughes D. W., McBride N., Wu. Z., 1993, MNRAS, 260, 43
Wu Z., Williams I. P., 1995, Planet. Space Sci., 43, 723
Wu Z., Williams I. P., 1996, MNRAS, 280, 1210

This paper has been typeset from a Microsoft Word file prepared by the author.